Macromolecules

ARTICLE

pubs.acs.org/Macromolecules

Viscoelasticity of Graphite Oxide-Based Suspensions in PDMS

Aline Guimont,[†] Emmanuel Beyou,[†] Grégory Martin,[‡] Philippe Sonntag,[§] and Philippe Cassagnau*[,†]

[†]Laboratoire Ingénierie des Matériaux Polymères, CNRS UMR 5223 Université de Lyon, F-69003, France Université Lyon1, Villeurbanne, F-69622 Lyon, France

[‡]Hutchinson Polymers, Parc d'Activités d'Arboria, 55 Rue des Platanes, 45700 Pannes, France

[§]Hutchinson S.A., Centre de Recherche, Rue Gustave Nourry, BP 31, 45120 Chalette-sur-Loing, France

ABSTRACT: The viscoelastic behavior of graphite oxide-loaded PDMS suspensions showed, at low frequencies, a dominant elastic behavior with the appearance of a secondary plateau above 1.5 wt %. Within the investigated concentrations, such behavior was not observed for the graphite and functionalized graphite oxide/PDMS suspensions. This low percolation threshold of GO sheets was attributed to a macroscale aggregation. Furthermore, the critical strain (transition between the linear and nonlinear regime) was observed to slightly depend on the particle concentration ($\gamma_c \propto \phi^{-1\pm0.2}$). Consequently, the exponent x ($x = 0.4$), related to the filler volume fraction and the aggregate structure, is lower than 1. This result means that a fractal structure cannot be associated with the aggregation of GO sheets. Actually, GO sheets aggregate into agglomerates that span through the gap between the plates of the rheometer. Agglomeration of GO sheets without any fractal structure explains this particular behavior. Furthermore, recovery tests consisting of subsequent strain sweep tests proved that the initial equilibrium network can be totally and rapidly restored. This particular behavior originates from the low viscosity of the PDMS suspension allowing Brownian motion of graphene oxide sheets to occur within only a few seconds.

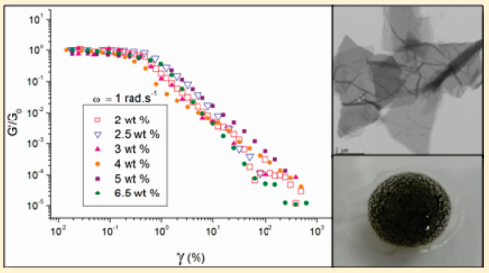

INTRODUCTION

Polymer nanocomposites have attracted considerable industrial and academic interest over the past few years because they often exhibit remarkable mechanical, thermal, electrical, and gas barrier properties.[1−3] Property enhancements originate from the nature of the nanofiller, e.g., their small size and their high aspect ratio, and have been attributed to the large interface areas between the nanofiller and the host polymer matrix. However, as the nanofillers are held together into stacky agglomerates, efforts have been done to separate the original stacks into individual layers and disperse them into polymers.[4−7] Recently, graphene-based materials have attracted much interest due to their remarkable properties and promising applications.[8,9] This great interest has been made obvious by the significant number of recent scientific papers and by the 2010 Nobel Prize in Physics, which was awarded to Andre Geim and Konstantin Novoselov for their pioneer work on isolated graphene sheets. Graphene is a two-dimensional sheet composed of sp^2 carbon atoms and is expected to have tensile modulus and ultimate strength values similar to those of single-walled carbon nanotubes (SWCNTs). The production of graphene sheets has been achieved in the literature by micromechanical cleavage of graphite,[10] sonication in the presence of *N*-methylpyrrolidone,[11] electrochemical functionalization of graphite,[12] and dissolution of graphite in chlorosulfonic acid.[13]

From an industrial application point of view, the most promising method for large-scale production of graphene is based on the oxidation of graphite leading to graphite oxide (GO), which can subsequently be functionalized, followed by its reduction to restore electrical conductivity. For example, Stankovich et al.[14] prepared graphene/polystyrene-based nanocomposites by solution mixing of exfoliated functionalized GO sheets. The electrical conductivity was restored by in situ chemical reduction of GO with dimethylhydrazine, leading to an electrical percolation threshold close to 0.1 vol %. However, a potential large-scale development of GO and graphene/polymer nanocomposites depends on the ability to homogeneously disperse these fillers in polymer matrices and to ensure strong GO− and graphene−polymer interfacial adhesion.

Indeed, GO and graphene sheets have a strong tendency to stack into dense clusters or scroll into tubes. Different strategies have then been developed to optimize their dispersions in thermoplastic polymers. For example, Kim et al.[15] showed that graphite exfoliation can be achieved from GO via thermal expansion or surface treatment with isocyanate, leading to the successful preparation of graphene and graphite oxide sheets/polyurethane nanocomposites with improved gas barrier properties and electrical conductivity. In fact, many different functional groups can be introduced onto the graphene oxide sheets by chemical modification of hydroxyl and epoxy groups created during the oxidation step.[16,17] Furthermore, polymer chain grafting onto graphene oxide sheets has also been investigated. For example, Yang et al.[18] prepared exfoliated graphene oxide sheets decorated with poly(2-(dimethylamino)ethyl methacrylate chains by using a grafting from ATRP procedure.

Received: January 13, 2011
Revised: March 13, 2011
Published: April 29, 2011

A direct consequence of incorporating GO in molten polymers is the significant change in viscoelastic and electrical properties. Compared with common microparticles, the 2D large aspect ratio of GO is expected to lead to the formation of a solidlike material at a relatively low GO concentration. The concentration onset, at which the viscoelastic and electrical properties dramatically change, is defined as the percolation threshold. Viscoelastic properties including the percolation threshold are extremely sensitive to how the nanofillers are dispersed.[19,20] The dispersion and the anisotropy (alignment or packing) of nanoparticles of high aspect ratio such as CNTs have a strong influence on the rheological, electrical, and mechanical properties of the nanocomposites. Actually, it is expected that the high aspect ratio of nanoparticles combined with intensive flows lead to the anisotropy of particle suspensions. Under flow, the particle orientation eliminates the particle−particle contacts breaking down the continuous network and leading to a decrease of electrical conduction and/or elastic behavior of nanocomposites as the particle orientation becomes more and more anisotropic. Such behavior for CNTs under polymeric flow has been recently described in detail by Bauhofer et al.[21] and Abbasi et al.[22] Regarding low-viscosity suspensions, a CNT aggregation mechanism was clearly evidenced. Such a phenomenon in Brownian suspensions has been recently reviewed by Hobbie.[23] Low shear deformations are well-known to induce an aggregation mechanism whereas high shear leads to a breakdown of the aggregates forming less entanglement.[24] Consequently, the viscoelastic behavior drastically changes depending on the aggregation state of the CNTs. However, can the GO suspensions obey the general trends observed for CNTs? Kim and Macosko[25] studied the processing−property relationships of polycarbonate/graphene nanocomposites. For injection and compression-molded samples, they observed flow-induced orientation of GO sheets. However, long-term annealing of the aforementioned samples allowed the GO sheets to recover a more random orientation. Furthermore, the viscoelastic behavior was observed to strongly depend on the nature of the particle. From the viscoelastic curves reported in this paper, it is clear that the percolation threshold of the functionalized graphene sheets is lower than the graphite one. However, as far as we know, no work has been reported on the suspension of graphite and GO in low-viscosity liquids. In fact, acknowledging that the diffusion coefficient of nanoparticles is inversely proportional to the fluid viscosity, low-viscosity fluid polymers should be selected if one wishes to observe aggregation/disaggregation phenomena in a short time scale.

In this paper, we report the rheology of PDMS-based suspensions with solvent-dispersed graphite oxide (GO) and decorated GO with 3-(acryloxypropyl)trimethoxysilane (GO-M) sheets. The aim is to study both the dispersion of these carbon nanofillers in PDMS fluids from viscoelastic measurements (Rouse regime) and their rearrangement in terms of complex shear modulus recovery under nonlinear deformation. Finally, the dispersion stability and aggregation/agglomeration structural formation of such 2D sheets are discussed.

EXPERIMENTAL SECTION

Materials. The polymer matrix is a poly(dimethyl-*co*-vinylmethyl)-siloxane trimethoxy-terminated, subsequently noted PDMS, purchased from ABCR. At room temperature, the low viscosity of this PDMS (e.g., η_0 = 0.6 Pa·s) allows the following PDMS/filler blends to be designated as suspensions.

The PDMS molar mass ($M \approx 10\,000$ g mol^{-1}) is much lower than the viscosity critical molar mass ($M_c \approx 30\,000$ g mol^{-1}).[26] Furthermore, in a recent paper, Gordon et al.[27] showed that from zero shear viscosity measurements on PDMS/polysilicate suspensions the critical molar mass M_c increases with particle loadings from M_c = 27 kg mol^{-1} to M_c = 33 kg mol^{-1}. Thus, one can assert that the low molar mass PDMS chains used in this current study are not entangled and obey the Rouse regime of relaxation.

Graphite powder was kindly provided by TIMCAL Graphite & Carbon (40 μm in size). Graphite oxide (GO) was synthesized from graphite powder using the Hummers' method.[28] A C/O atomic ratio of 2.22 was determined by elemental analysis. Potassium permanganate ($KMnO_4$), sodium nitrate ($NaNO_3$), concentrated sulfuric acid (H_2SO_4), and *N*-methylpyrrolidone (NMP) were all purchased from Aldrich. 3-(Acryloxypropyl)trimethoxysilane (APTMS) was purchased from ABCR.

Preparation of Functionalized Graphite Oxide with 3-(Acryloxypropyl)trimethoxysilane (GO-M). Graphite oxide (130 mg) was dispersed in 3-(acryloxypropyl)trimethoxysilane (1.25 mg, 5.3 mmol) using an ultrasound bath (15 min). 6.5 mL of *N*-methylpyrrolidone was then added. The mixture underwent a second dispersion cycle of 30 min in an ultrasound bath. The dispersion was then allowed to stir and to heat for 4 h at 110 °C. The product was purified by centrifugation in methanol, water, and acetone. The product was then dried overnight at 80 °C under vacuum.

Preparation of PDMS/Graphene Oxide-Based Suspensions. PDMS was dissolved in THF and in toluene for GO and GO-M-based suspensions respectively in order to prepare loaded suspensions of 1−6.5 wt %. A predetermined amount of GO and of GO-M was dispersed in THF at 0.6 wt % and toluene at 0.3 wt %, respectively, by sonication and then mixed with the corresponding PDMS solution. The resulting mixtures were mechanically stirred for 1 h and then poured in a Petri dish to dry. The targeted loading of the blend (filler−PDMS−solvent) was 10 wt %. The graphite-based suspensions were prepared following the same procedure.

Characterizations. FTIR spectra were recorded on a Nicolet FTIR 460 spectrometer using powder-pressed KBr pellets. Specimens for the measurements were prepared by mixing 1 mg of the sample powder with 150 mg of KBr and by pressing the mixture into pellets. FTIR spectra were obtained at a resolution of 6.0 cm^{-1} at room temperature in a wavenumber range between 4000 and 400 cm^{-1} and averaged over 50 scans.

The powder X-ray diffraction (XRD) measurements were performed on a Siemens D500 diffractometer (Ni-filtered Cu KR radiation, 1.5405 Å). The $d_{(002)}$ basal spacings were calculated from the 2θ values using the EVA software.

TGA was carried out with a Mettler TG 50/TA 3000 thermobalance, controlled by a TC10A microprocessor. Samples were heated at 5 °C min^{-1} under helium flow (20 mL min^{-1}).

TEM analysis was performed on a Philips CM120 electron microscope operating at 80 kV in the "Centre Technologique des Microstructures de l'Université Lyon 1". In a typical experiment, one drop of the colloidal dispersion was deposited on a carbon film supported by a copper grid and allowed to air-dry before observation.

The viscoelastic measurements were carried out on the dynamic rheometer (RMS 800 from Rheometrics) at room temperature ($T \approx$ 22 °C). Most of the rheological measurements were performed in an oscillatory shear mode ($0.1 \leq \omega$ (rad s^{-1}) ≤ 100). The gap between the plates was fixed at 0.8 mm. The testing of nonlinear behavior of all the suspensions was performed using the strain rheometer in the range of deformation from 0.02 to 200%.

RESULTS AND DISCUSSION

Grafting of APTMS onto GO (GO-M). Using flake graphite as a starting material to synthesize GO requires strong chemical

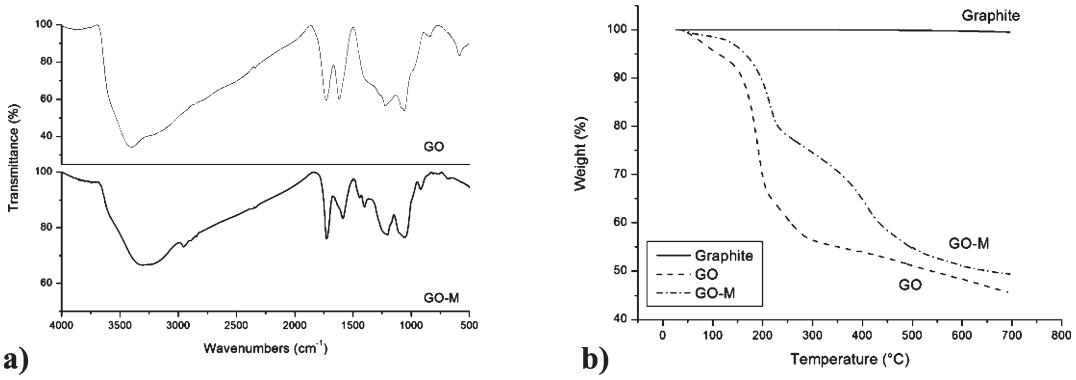

Figure 1. Characterization and titration of APTMS grafting onto GO (GO-M). (a) FTIR spectra of GO before and after APTMS grafting (GO-M). (b) TGA curves of pristine graphite, unmodified GO and GO-M.

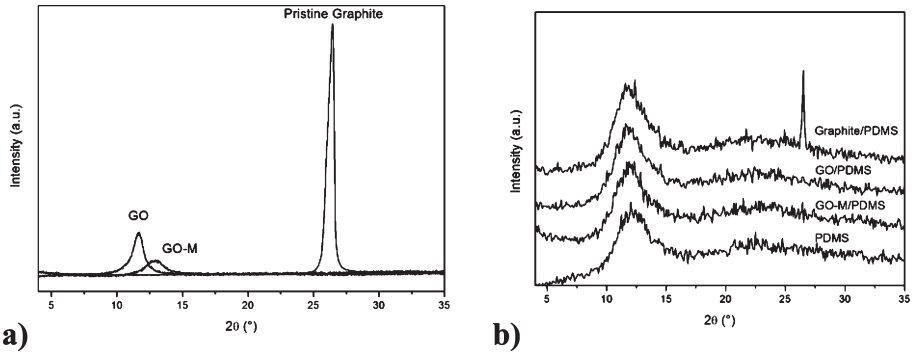

Figure 2. X-ray patterns of graphite, GO, and GO-M: (a) dry powders, (b) in PDMS suspensions (particle weight fraction: 4 wt %). Intensity profiles are vertically shifted for clarity.

oxidants such as potassium permanganate and sulfuric acid, according to the experimental procedure of Tung.[29] Graphite oxide is composed of graphene oxide sheets stacked with an interlayer spacing between 6 and 10 Å depending on the water content.[30] Its structure is mostly described as built of pristine aromatic islands separated from each other by aliphatic regions containing epoxide and hydroxyl groups and double bonds with carbonyl functional groups at the edges.[9]

The treatment of GO with organic alkoxysilanes (e.g., acryloxypropyltrimethoxysilane (APTMS)) can lead to the derivatization of both the edge carboxyl and surface hydroxyl functional groups. Indeed, it is well-known that the trimethoxysilyl group of APTMS, a commercially available monomer, is very sensitive to water moisture and hydrolyzes very easily.[31,32] Therefore, it can be grafted onto edge carboxyl and surface hydroxyl functional groups of graphite oxide by hydrolysis/condensation reactions according to the sol−gel process. Moreover, the acryloxy group of APTMS may react with radical initiators and monomers to graft polymer chains from the graphite oxide surface or with polymethylhydrogenosiloxane by a catalytic hydrosilylation reaction. First of all, we qualitatively evidenced the grafting of APTMS onto graphite oxide by FTIR analysis. Figure 1a compares the FTIR spectra of GO before and after the grafting reaction with APTMS (GO-M). Characteristic vibrations of the carbonyl ($\upsilon_{C=O}$, 1730 cm^{-1}) and the aliphatic (υ_{C-H}, 2900−2800 cm^{-1}) groups of the APTMS compound clearly attest for the presence of APTMS on the graphite oxide surface. Moreover, the FTIR spectrum of the hydroxyl region of GO exhibits a strong and wide OH stretching vibration band in the range 3600−3100 cm^{-1} due to physisorbed water whereas the GO-M one displays a less stronger OH stretching vibration band due to grafting.

A quantitative approach by thermal gravimetric analysis (TGA) allowed us to accurately determine the grafting density of the APTMS units on the surface. TGA curves of unmodified GO and GO-M were recorded in the helium atmosphere (Figure 1b). GO shows decomposition peaks at 200 and 500 °C representing decomposition of oxygen functionality and sp^2, sp^3 carbon atoms, respectively. Organic compounds are well-known to decompose before 500 °C; therefore, the amount of grafted APTMS on GO-M can be calculated from the TGA data by measuring the weight loss observed in the temperature range 200−500 °C (Figure 1b). The decomposition temperature of the grafted APTMS, corresponding to the maximum of the derivative, is observed at 410 °C.

We obtained a weight loss of 15% which corresponds to 0.8 mmol of grafted silane per gram of GO-M or in other words one silane group per 89 carbon atoms which is close to the values given in the literature for the grafting of a series of azide compounds.[33] For example, He et al.[33] reported a value of around 1 mmol g^{-1} for the grafting of an azide-terminated ATRP initiator. However, grafting reactions of silane are very sensitive to experimental conditions (moisture content, silane chemical composition and functionality, washing procedures and curing treatments, etc.),[34,35] making it difficult to ensure reproducible results which may account for the large disparity of literature data (e.g., 3.8 mmol g^{-1} for 3-aminopropyldiethoxymethylsilane).[35]

The X-ray diffraction patterns of pristine graphite, GO, and GO-M are plotted in Figure 2a. A sharp peak centered around

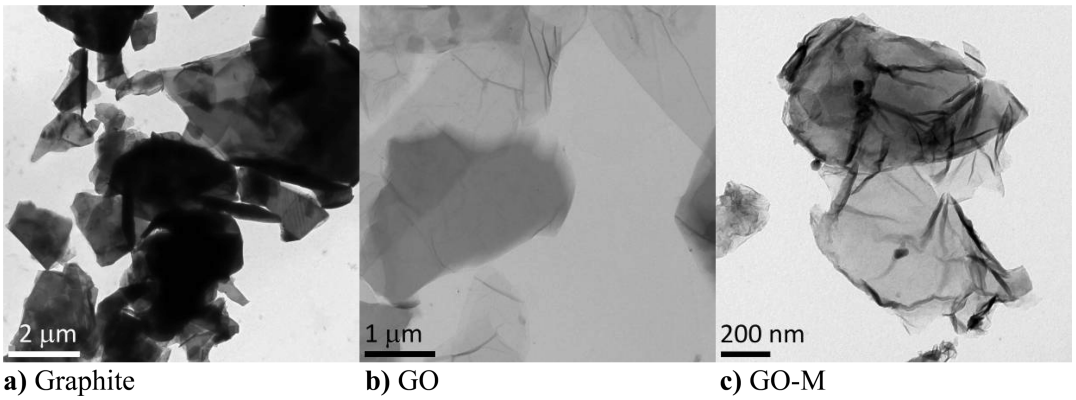

Figure 3. TEM images of dried particles: (a) graphite, (b) graphite oxide, and (c) graphite oxide decorated with 3-(acryloxypropyl)trimethoxysilane.

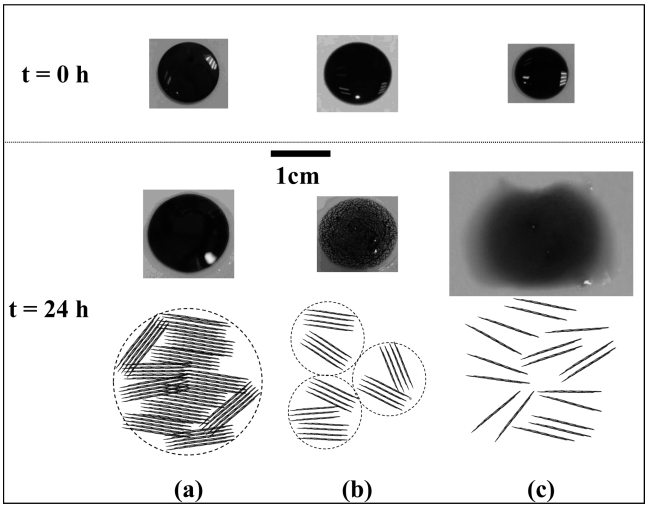

Figure 4. Visual observation of PDMS-based droplets (upper pictures: t = 0 h) after a 24 h rest period: (a) graphite, (b) graphite oxide, and (c) graphite oxide decorated with 3-(acryloxypropyl)trimethoxysilane. The scheme is a representation of the filler morphology (see hereinafter discussion).

2θ = 26.4° attributable to a high degree of ordering is observed for pristine graphite. This peak originates from the interlayer (002) spacing (d = 3.4 Å) according to Bragg's law. Upon oxidation of graphite (GO) and post-modification of GO (GO-M), the diffraction peak shifted toward lower angles (2θ = 11.7° and 12.9°, respectively) which asserts for an increase of the interlayer distance of the graphene oxide sheets of ~4 Å. GO exhibits an hygroscopic behavior generated by the presence of oxygen functions on its surface (atomic ratio C/O = 2.22, determined by elemental analysis). Thus, its interlayer distance strongly depends on its level of hydration.[30,36] The modified GO (GO-M) is less hydrophilic leading to a decrease of the interlayer distance. This interlamellar spacing is of the same order of magnitude as that reported in the literature for the grafting of aniline into graphite oxide.[37]

Beigbeder et al.[38] have recently reported a particular behavior of multiwall carbon nanotubes (MWCNTs) dispersed in low-viscosity PDMS (Rouse regime). On the basis of molecular dynamic simulations, the authors accessed the adsorption properties of polydimethylsiloxane chains (PDMS) on the external walled surface of MWNTs at the microscopic level. It was found that the physical adsorption of PDMS chains onto the CNT walls is mostly triggered by CH−π interactions between part of the PDMS methyl groups and the π-electron-rich surface of CNTs. Such interactions may lead to an individual separation of CNTs in PDMS which is equivalent to an exfoliation process.[39] CNT and graphite display similar chemical compositions; therefore, the stabilization of graphite sheets in PDMS suspensions can be assumed from specific interactions between PDMS methyl groups and the π-electron-rich surface of graphite according to the work of Biegbeder et al.[38] However, no exfoliation of graphite to graphene sheets from PDMS chains diffusion has been observed. Yet, the intercalation of graphite via oxidative treatment and exfoliation in PDMS suspension is expected. Nevertheless, in PDMS, the high hydrophilicity of GO, caused by the presence of oxygen functions on its surface, leads to the agglomeration of GO sheets. Unfortunately and according to Figure 2b, the X-ray noise of pure PDMS in the range 10° < 2θ < 15° does not allow us to conclude precisely about the exfoliation extent of GO and GO-M in liquid PDMS.

Morphological Characterization. Figure 3 shows the TEM images of the original graphite particles, GO, and GO-M samples cast from dilute THF, water, and toluene suspensions, respectively. The TEM micrograph of graphite shows thick stacked sheets of different sizes (Figure 3a). These agglomerates are partly destroyed after oxidation (Figure 3b), and GO appears partially transparent with typical large crumpled thin flakes, as already described by He.[33] After functionalization, the morphology of GO-M does not significantly change.

The visual observation of droplets (V = 26.5 ± 7.1 μL, at 3.9 wt %) deposited on a horizontal glass slide leads to some relevant conclusions about these suspensions (Figure 4). After a 24 h rest period, it can be observed in Figure 4c that the GO-M/PDMS droplet spreads over the glass slide, whereas the GO/PDMS one shows a yield stress liquid behavior (Figure 4b). The latter droplet is slightly deformed and the aggregation of GO particles can be clearly observed inside the droplet (Figure 4b).

Linear Viscoelasticity. As pointed out by many authors, linear viscoelasticity is an effective tool for understanding the particle dispersion and/or aggregation in filled polymer systems under molten conditions. Figure 5 shows the variation of the shear storage modulus and absolute complex viscosity of the different PDMS-based suspensions as a function of frequency. The storage modulus is extremely noisy at low frequencies (ω < 1 rad s^{-1}) due to the low value of the applied linear deformation. However, it can be clearly observed that the linear viscoelastic behavior of

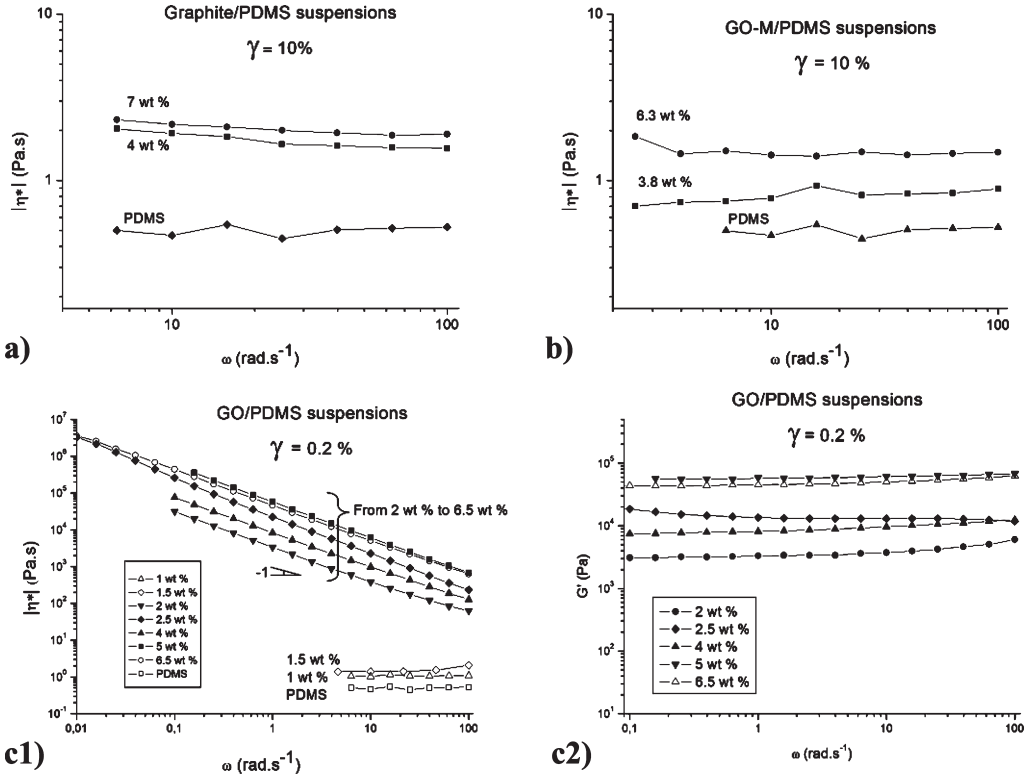

Figure 5. Absolute complex viscosity of PDMS suspensions at different weight fractions: (a) graphite, (b) graphite oxide decorated with 3-(acryloxypropyl)trimethoxysilane; (c1) graphite oxide; (c2) storage modulus variation of GO/PDMS suspensions.

graphite/PDMS and GO-M/PDMS suspensions (Figure 5, a and b, respectively) is not influenced by the frequency (the suspension is still Newtonian). In addition, this behavior stays valid for all particle concentrations. This result means that the interactions between graphite particles or GO-M particles are too low owing to their microsize scale. The graphite particles in the PDMS suspensions mainly undergo the force of gravity explaining their decantation, which was visually observed after a few days rest. On the contrary, the GO-M suspensions are totally stable. Indeed, no decantation or agglomeration was observed. A priori, the characteristic size of the GO-M particles determined from TEM analysis is at the submicrometer scale. Therefore, the surface functionalization with 3-(acryloxypropyl)trimethoxysilane of these submicrometer particles prevents their aggregation by screening the depletion forces. The dominant force in the present case is the repulsion force between the submicrometer particles.

Unlike the graphite/PDMS and GO-M/PDMS suspensions, the GO/PDMS ones show a drastic change in the viscoelastic properties. In other words, the GO/PDMS suspensions show a solid-like behavior response which includes a non-terminal zone of relaxation leading to apparent yield stress, as already visually observed from the non-deformation of a droplet (Figure 4b). More precisely, Figure 5c1 shows a yield stress behavior ($|\eta^*(\omega)| \propto \omega^{-1}$), and Figure 5c2 hence reveals that the terminal relaxation zone (variation of the storage modulus G') of the suspensions has been strongly altered. Actually, for GO concentrations higher than 1.5 wt %, the viscoelastic behavior does not show any terminal flow zone, unlike the suspensions with lower filler loading (<1.5 wt %). Moreover, at low frequencies, the elastic character of these suspensions becomes dominant with the appearance of a secondary plateau ($G_0 = \lim_{\omega \to 0} G'(\omega)$) which obeys the following power law dependence on particle concentration, $G_0 \propto \phi^{2.5 \pm 0.2}$.

Note that this viscoelastic transition does not occur for graphite/PDMS (Figure 5a) and GO-M/PDMS (Figure 5b) suspensions at least with weight fractions not higher than 7 and 6.3 wt %, respectively. Such behavior at low particle concentration has been extensively reported for polymer nanocomposites. Compared with spherical particles, particles with shape anisotropy and high aspect ratio (platelets, sheets, rods) percolate at smaller weight fractions. Furthermore, it is generally admitted that the association of particles into a fractal structure seems more compatible for low percolation threshold than the random distribution of isolated particles finely dispersed and stabilized in the liquid medium. Such behavior is well-known for carbon nanotubes[21,24] in their semidilute regime. Note that a general review was addressed by Hobbie[23] on the aggregation mechanisms under shear for carbon nanotube suspensions. Regarding rheology of disk suspensions, Mongondry et al.[40] and Loiseau and Tassin[41] first reported a possible aggregation mechanism of disk particles, i.e., laponite. For example, they observed that five hours were necessary to achieve an equilibrium behavior of the suspension,[41] i.e., a constant value of the complex shear modulus. More recently, Kim and Macosko[25] observed that the storage modulus of polycarbonate/graphene nanocomposites increases with annealing time over a few hours. The authors explained this phenomenon by the increased effective volume of rotating disk and the restoration of an elastic network which was broken down by the squeezing flow during sample loading. However, Kim and Macosko[25] did not suspect any aggregation effect of graphene particles.

Assuming that graphene sheets behave as Brownian particles, the rotary diffusivity D_r of a circular Brownian disk (diameter: d)

can be expressed from the Stokes−Einstein law according to

$$D_r = \frac{3kT}{4\eta d^3} \quad (1)$$

Using the same figures than Kim and Macosko[25] for graphene sheets and a viscosity of 0.6 Pa·s for the PDMS matrix, the rotational relaxation time is $1/D_r \approx 15$ s. This oversimplified calculation means that the graphene particles are able to recover their random orientation in a few seconds after their anisotropic orientation under flow. Finally, our results suggest an aggregation mechanism of GO sheets in PDMS as suspected by Loiseau and Tassin[41] for laponite in low molecular mass poly(ethylene oxide). Furthermore, as visually observed in Figure 4b, this aggregation develops at a large scale with a magnitude order of millimeter. Actually, this aggregation network spans through the gap between the parallel plates of the rheometer. To conclude, the low percolation threshold of GO sheets is due to their aggregation at a macroscale under the driving force of their Brownian motion. Such mechanism is the dominant one in low viscous suspensions in the dilute regime for which the relaxation Brownian time is in the same order of the characteristic time of the experiment. On the contrary, for high viscous systems ($\eta > 100$ Pas) a randomization mechanism such as aging colloidal glasses can be investigated in polystyrene/layers silicates[42] and polycarbonate/graphene nanocomposites.[25] However, this type of experiment in molten conditions is constrained by the thermal stability of the polymer.

According to Ren et al.,[43] the weight fraction of layered particles at the percolation threshold can be calculated from the basis of percolating spheres. The expression derived by Ren et al.[43] can be simplified when considering low weight fraction of particles (eq 2)[41]

$$w_g \approx \frac{3\phi_{per}h}{4R}\frac{\rho_g}{\rho_{PDMS}} \quad (2)$$

where ϕ_{per} (=0.3) is the volume fraction at the percolation concentration of randomly distributed spheres and h and R are the thickness and the particle radius, respectively. ρ_g and ρ_{PDMS} are the densities of graphite and PDMS, respectively. According to Kim and Macosko,[25] the particle aspect ratio $A_f = 2R/h$ of GO particles in PDMS can then be calculated from the weight fraction at the percolation w_g (eq 3).

$$A_f = \frac{3\Phi_{per}}{2w_g}\frac{\rho_g}{\rho_{PDMS}} \quad (3)$$

Herein, assuming $w_g \approx 0.015$ and $\rho_g/\rho_{PDMS} \approx 2$, we finally found $A_f \approx 60$. This value is close to the value calculated by Kim and Macosko[25] for functionalized graphene sheets dispersed in polycarbonate ($A_f \approx 90$). However, this value is overestimated in our present work since the GO sheets aggregate resulting in a lower percolation threshold.

Nonlinear Viscoelasticity. Only few works have recently been reported on the nonlinearity of polymer nanocomposites.[19] Regarding graphene-based polymer nanocomposites, Kim and Macosko[25] studied the variation of the storage modulus versus strain in order to determine the transition between the linear and nonlinear regime. As expected, the decrease in yield strain becomes more pronounced from a critical weight fraction (e.g., 3 and 5 wt % for graphite and between 1 and 1.5 wt % for functionalized graphite oxide). Actually, this critical weight fraction depends on the graphene surface treatment and consequently on the particle aspect ratio A_f. In our present work,

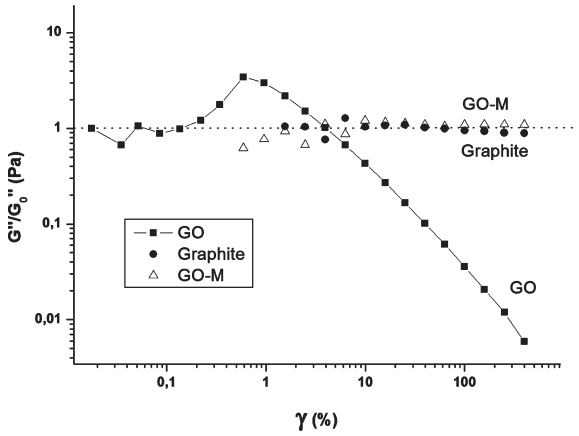

Figure 6. Variation of the normalized loss modulus (G''/G_0'') versus strain for a weight concentration of 4 wt % ($\omega = 1$ rad s^{-1}). Graphite and GO-M suspensions do not show any nonlinear effect in this strain range.

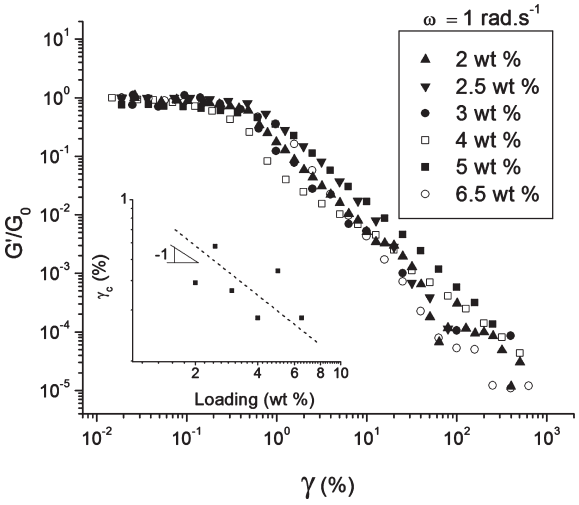

Figure 7. Variation of the normalized storage modulus (G'/G_0') versus strain for different GO weight fractions: 2, 2.5, 3, 4, 5, and 6.5% ($\omega = 1$ rad s^{-1}).

Figure 6 shows that the graphite and GO-M suspensions are linear throughout the entire investigated strain domain (from 0.1 to 600% at 1 rad s^{-1}). It must be pointed out that the variation of the loss modulus has been plotted because the variation of the storage modulus is too noisy, in particular for graphite and GO-M suspensions. Regarding the GO/PDMS suspension, the deviation from the linear viscoelastic behavior starts at low strains ($\gamma_c \approx 0.2\%$ at the highest concentration in GO), showing a strong nonlinear effect for this suspension. Furthermore, it can be observed that loss modulus goes through a maximum as generally observed for filled polymer systems. Aranguren et al.[44] assumed that the maximum in G'' is related to the energy dissipation produced by the breaking down of filler aggregates (in their case silica). This maximum thus depends on the dispersion state.

Furthermore, Figure 7 shows that the transition between the nonlinear and linear regime slightly depends on GO concentration. This transition obeys the following power law dependence $\gamma_c \propto \phi^{-1\pm0.2}$ as shown in Figure 7.

Actually, many works in the literature showed that two power laws can be distinguished $\gamma_c \propto \phi^{-2}$ and $\gamma_c \propto \phi^{-1}$ for fumed silica

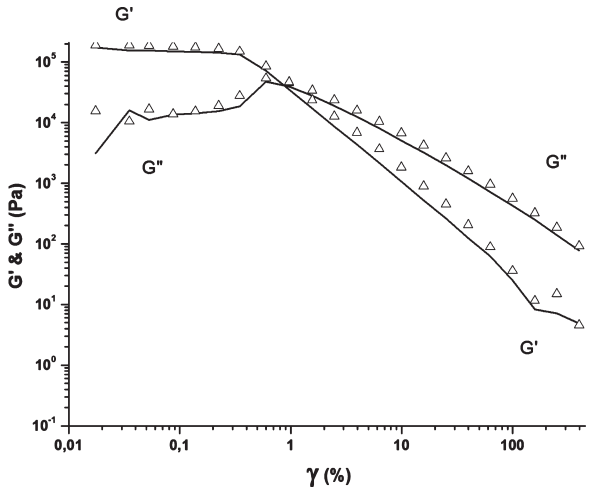

Figure 8. Experiment of moduli recovery evidenced by a subsequent strain sweep test preceded by an identical nonlinear test ($\omega = 1$ rad s^{-1}). GO weight fraction: 4 wt %. Full line: first strain sweep. Symbols: subsequent nonlinear test.

and organo-clays nanocomposites, respectively. However, note that these power exponents are extremely sensitive to the experimental criteria used by the authors. To our knowledge, regarding graphene nanocomposites, only Kim and Macosko[25] explored the limit of linearity graphene/polycarbonate composites. From their results we can derive the following power law: $\gamma_c \propto \phi^{-4}$. Generally speaking, the decrease of linear viscoelastic properties in nanocomposite polymers originates from the difference in the degree of dispersion and more precisely the degree of layer exfoliation. From a physical point of view, this result is of importance as it shows that the linear viscoelastic properties of nanocomposites are governed by the particle−particle interaction of the physical network. According to the work of Shih and co-workers[45] focusing on fractal systems, the value of the plateau modulus and critical strain can be predicted by the following power laws: $G_0 \propto \phi^{(3+x)/(3-d_f)}$ and $\gamma_c \propto \phi^{-(1+x)/(3-d_f)}$, respectively. In these equations d_f is the fractal dimension of the aggregate network and x is an exponent related to the filler volume fraction and the aggregate structure. The exponent x depends on the number of layer particles per aggregate and is thus related to the degree of exfoliation. According to our experimental results, we obtained the following power laws: $G_0 \propto \phi^{2.5\pm0.2}$ (Figure 5c2) and $\gamma_c \propto \phi^{-1\pm0.2}$ (Figure 7), leading to $d_f = 1.7 \pm 0.3$ and $x = 0.4 \pm 0.4$. These denominations (d_f and x) have been used in the literature[46,47] to discuss clay dispersion with various fractal structures. It should be noted that these values have considerable uncertainty due to the experimental determination of the power laws on G_0 and γ_c. Low values of d_f suggest better particle dispersion with a more open fractal structure. However, for spherical spheres, the exponent x must exceed 1 for percolation to occur. The conclusions of Vermant et al.[46] can be extrapolated to graphene-layered nanocomposites: x is representative of a local aggregate structure, which is not fractal. According to this discussion and more generally from the linear and nonlinear behavior of the viscoelastic behavior of PDMS suspensions, a 2D scheme of graphite, GO, and GO-M based PDMS suspensions has been drawn in Figure 4.

Finally, another important aspect in the mechanisms involved in the nonlinear viscoelasticity of nanocomposites is the moduli restoration following the network destruction by a large strain perturbation. Different kinds of rheological experiments were used to quantify this thixotropic effects resulting from the presence of nanofillers. For example, Figure 8 shows a subsequent strain sweep experiment immediately performed on GO/PDMS suspensions right after the first nonlinear test. Then, the complex shear modulus behavior in the linear domain evidence a network structure of GO sheets. We demonstrated that this network was formed by the agglomeration of nonfractal GO sheets. The increase of the strain amplitude, up to 100%, leads to a high modification of this network structure out of this equilibrium state. Furthermore, this figure clearly shows that the nonlinear effect is a reversible process, and the GO/PDMS suspension undergoes a total renewal of its original equilibrium structure. This phenomenon, generally called thixotropy, can actually be considered as a kind of viscoelasticity but with typical relaxation times of a few hours for polymeric system of high viscosity.[48] However, in the present case, the recovery time is on the magnitude order of a few seconds according to the rotary diffusion of GO sheets in low viscous PDMS. Furthermore, it can be concluded that the nonlinearity effect of GO/PDMS suspensions is governed by the network breakdown of agglomerated GO particles (particle−particle interaction).

CONCLUSION

Graphite, graphite oxide (GO), and graphite oxide functionalized with 3-(acryloxypropyl)trimethoxysilane (GO-M) were dispersed in low molar mass PDMS (no entangled chains, viscosity: $\eta = 0.6$ Pa·s). These suspensions have been characterized from a linear and nonlinear viscoelasticity point of view. First of all, transmission electron microscopy and X-ray diffraction showed an intercalated morphology of graphite oxide potentially exfoliated in the PDMS suspension. Furthermore, it was noticed in this study that the grafting of APTMS onto GO sheets prevents their particle−particle interaction and consequently their agglomeration.

Only the PDMS suspension filled with the graphite oxide showed a drastic change in the viscoelastic properties for weight fractions up to 6.5 wt %. Actually, for GO concentrations higher than 1.5 wt %, the viscoelastic behavior does not show any terminal flow zone and the elastic character of this suspension becomes dominant at low frequencies with the appearance of a secondary plateau. Furthermore, the low percolation threshold of GO sheets is attributed to their macroscale aggregation/agglomeration driven by their Brownian motion in these low-viscosity PDMS suspensions. It was further concluded that the surface modification of graphite oxide by 3-(acryloxypropyl)trimethoxysilane prevents the aggregation of GO sheets.

The nonlinear behavior of the GO/PDMS suspensions revealed that the increase of strain amplitude leads to a high modification of the network structure out of the equilibrium state. Moreover, the critical strain (transition between the linear and nonlinear regime) was observed to slightly depend on the particle concentration ($\gamma_c \propto \phi^{-1\pm0.2}$). Consequently, the exponent x related to the filler volume fraction and the aggregate structure is lower than 1 ($x = 0.4 \pm 0.4$). This result means that a fractal structure cannot be associated with the aggregation of GO sheets. Actually, GO sheets aggregate into agglomerates that span through the gap between the plates of the rheometer. Finally, recovery tests carried out by subsequent strain sweep proved that the initial equilibrium network structure can be completely and instantaneously restored, and this within the time

necessary to start the subsequent nonlinear test, i.e., a few seconds. Compared with literature works, this particular behavior originates from the low viscosity of the suspension that allows Brownian motion of graphite oxide sheets within the magnitude order of a few seconds.

Future work will consist in grafting polymethylhydrogensiloxane onto APTMS-grafted GO sheets in order to check if functionalization with a polysiloxane backbone offers the possibility to tailor the viscoelastic properties of GO/PDMS suspensions.

AUTHOR INFORMATION

Corresponding Author

*E-mail: Philippe.cassagnau@univ-lyon1.fr.

ACKNOWLEDGMENT

This study was carried out in the framework program of the ANR MACOPHENE. We would personally like to thank Pierre Alcouffe and all the staff of the Technological Centre of Microstructures of the University of Lyon 1 for their technical help.

REFERENCES

(1) Podsiadlo, P.; Kaushik, A. K.; Arruda, E. M.; Waas, A. M.; Shim, B. S.; Xu, J. D.; Nandivada, H.; Pumplin, B. G.; Lahann, J.; Ramamoorthy, A.; Kotov, N. A. *Science* **2007**, *318*, 80–83.

(2) Moniruzzaman, M.; Winey, K. I. *Macromolecules* **2006**, *39*, 5194–5205.

(3) Okada, A.; Usuki, A. *Macromol. Mater. Eng.* **2006**, *291* 1449–1476.

(4) Bailly, B.; Donnenwirth, A. C.; Bartholome, C.; Beyou, E.; Bourgeat-Lami, E. *J. Nanomater.* **2006**, Sp Issue, 76371, DOI: 10.1155/JNM/2006/76371.

(5) Konn, C.; Morel, F.; Beyou, E.; Chaumont, P.; Bourgeat-Lami, E. *Macromolecules* **2007**, *40*, 7464–7472.

(6) Akbar, S.; Beyou, E.; Cassagnau, P.; Chaumont, P.; Farzi, G. *Polymer* **2009**, *50*, 2535–2543.

(7) Rybak, A.; Warde, M.; Beyou, E.; Chaumont, P.; Bechelany, M.; Brioude, A.; Toury, B.; Cornu, D.; Miele, P.; Guiffard, B.; Seveyrat, L.; Guyomar, D. *Nanotechnology* **2010**, *21* (14), 145610, DOI: 10.1088/0957-4484/21/14/145610.

(8) Allen, M. J.; Tung, V. C.; Kaner, R. B. *Chem. Rev.* **2010**, *110*, 132–145.

(9) Kim, H.; Abdala, A. A.; Macosko, C. W. *Macromolecules* **2010**, *43*, 6515–6530.

(10) Novoselov, K. S.; Geim, A. K.; Morozov, S. V.; Jiang, D.; Zhang, Y.; Dubonos, S. V.; Grigorieva, I. V.; Firsov, A. A. *Science* **2004**, *306*, 666–669.

(11) Hernandez, Y.; Nicolosi, V.; Lotya, M.; Blighe, F. M.; Sun, Z. Y.; De, S.; McGovern, I. T.; Holland, B.; Byrne, M.; Gun'ko, Y. K.; Boland, J. J.; Niraj, P.; Duesberg, G.; Krishnamurthy, S.; Goodhue, R.; Hutchison, J.; Scardaci, V.; Ferrari, A. C.; Coleman, J. N. *Nature Nanotechnol.* **2008**, *3*, 563–568.

(12) Liu, N.; Luo, F.; Wu, H. X.; Liu, Y. H.; Zhang, C.; Chen, J. *Adv. Funct. Mater.* **2008**, *18*, 1518–1525.

(13) Behabtu, N.; Lomeda, J. R.; Green, M. J.; Higginbotham, A. L.; Sinitskii, A.; Kosynkin, D. V.; Tsentalovich, D.; Parra-Vasquez, A. N. G.; Schmidt, J.; Kesselman, E.; Cohen, Y.; Talmon, Y.; Tour, J. M.; Pasquali, M. *Nature Nanotechnol.* **2010**, *5*, 406–411.

(14) Stankovich, S.; Dikin, D. A.; Dommett, G. H. B.; Kohlhaas, K. M.; Zimney, E. J.; Stach, E. A.; Piner, R. D.; Nguyen, S. T.; Ruoff, R. S. *Nature* **2006**, *442*, 282–286.

(15) Kim, H.; Miura, Y.; Macosko, C. W. *Chem. Mater.* **2010**, *22*, 3441–3450.

(16) Lerf, A.; He, H. Y.; Forster, M.; Klinowski, J. *J. Phys. Chem. B* **1998**, *102*, 4477–4482.

(17) Dreyer, D. R.; Park, S.; Bielawski, C. W.; Ruoff, R. S. *Chem. Soc. Rev.* **2010**, *39*, 228–240.

(18) Yang, Y.; Wang, J.; Zhang, J.; Liu, J.; Yang, X.; Zhao, H. *Langmuir* **2009**, *25*, 11808–11814.

(19) Cassagnau, P. *Polymer* **2008**, *49*, 2183–2196.

(20) Jancar, J.; Douglas, J. F.; Starr, F. W.; Kumar, S. K.; Cassagnau, P.; Lesser, A. J.; Sternstein, S. S.; Buehler, M. J. *Polymer* **2010**, *51*, 3321–3343.

(21) Bauhofer, W.; Schulz, S. C.; Eken, A. E.; Skipa, T.; Lellinger, D.; Alig, I.; Tozzi, E. J.; Klingenberg, D. J. *Polymer* **2010**, *51*, 5024–5027.

(22) Abbasi, S.; Carreau, P. J.; Derdouri, A. *Polymer* **2010**, *51*, 922–935.

(23) Hobbie, E. K. *Rheol. Acta* **2010**, *49*, 323–334.

(24) Moreira, L.; Fulchiron, R.; Seytre, G.; Dubois, P.; Cassagnau, P. *Macromolecules* **2010**, *43*, 1467–1472.

(25) Kim, H.; Macosko, C. W. *Polymer* **2009**, *50*, 3797–3809.

(26) Ressia, J. A.; Villar, M. A.; Valles, E. M. *Polymer* **2000**, *41*, 6885–6894.

(27) Gordon, G. V.; Schmidt, R. G.; Quintero, M.; Benton, N. J.; Cosgrove, T.; Krukonis, V. J.; Williams, K.; Wetmore, P. M. *Macromolecules* **2010**, *43*, 10132–10142.

(28) Hummers, W. S.; Offeman, R. E. *J. Am. Chem. Soc.* **1958**, *80*, 1339.

(29) Tung, V. C.; Allen, M. J.; Yang, Y.; Kaner, R. B. *Nature Nanotechnol.* **2009**, *4*, 25–29.

(30) Park, S.; Ruoff, R. S. *Nature Nanotechnol.* **2009**, *4*, 217–224.

(31) Ozaki, H.; Hirao, A.; Nakahama, S. *Macromolecules* **1992**, *25*, 1391–1395.

(32) Gamys, C. G.; Beyou, E.; Bourgeat-Lam, E. *J. Polym. Sci., Part A: Polym. Chem.* **2010**, *48*, 784–793.

(33) He, H. K.; Gao, C. *Chem. Mater.* **2010**, *22*, 5054–5064.

(34) Matsuo, Y.; Tabata, T.; Fukunaga, T.; Fukutsuka, T.; Sugie, Y. *Carbon* **2005**, *43*, 2875–2882.

(35) Matsuo, Y.; Nishino, Y.; Fukutsuka, T.; Sugie, Y. *Carbon* **2007**, *45*, 1384–1390.

(36) Liu, Z. H.; Wang, Z. M.; Yang, X. J.; Ooi, K. T. *Langmuir* **2002**, *18*, 4926–4932.

(37) Zhang, K.; Zhang, L. L.; Zhao, X. S.; Wu, J. S. *Chem. Mater.* **2010**, *22*, 1392–1401.

(38) Beigbeder, A.; Linares, M.; Devalckenaere, M.; Degee, P.; Claes, M.; Beljonne, D.; Lazzaroni, R.; Dubois, P. *Adv. Mater.* **2008**, *20*, 1003–1007.

(39) Marceau, S.; Dubois, P.; Fulchiron, R.; Cassagnau, P. *Macromolecules* **2009**, *42*, 1433–1438.

(40) Mongondry, P.; Nicolai, T.; Tassin, J. F. *J. Colloid Interface Sci.* **2004**, *275*, 191–196.

(41) Loiseau, A.; Tassin, J. F. *Macromolecules* **2006**, *39*, 9185–9191.

(42) Ren, J. X.; Casanueva, B. F.; Mitchell, C. A.; Krishnamoorti, R. *Macromolecules* **2003**, *36*, 4188–4194.

(43) Ren, J. X.; Silva, A. S.; Krishnamoorti, R. *Macromolecules* **2000**, *33*, 3739–3746.

(44) Aranguren, M. I.; Mora, E.; Degroot, J. V.; Macosko, C. W. *J. Rheol.* **1992**, *36*, 1165–1182.

(45) Shih, W. H.; Shih, W. Y.; Kim, S. I.; Liu, J.; Aksay, I. A. *Phys. Rev. B* **1990**, *42*, 4772–4779.

(46) Vermant, J.; Ceccia, S.; Dolgovskij, M. K.; Maffettone, P. L.; Macosko, C. W. *J. Rheol.* **2007**, *51*, 429–450.

(47) Durmus, A.; Kasgoz, A.; Macosko, C. W. *Polymer* **2007**, *48*, 4492–4502.

(48) Larson, R. G. Particles in viscoelastic liquids: "Filled melts". In *The Structure and Rheology of Complex Fluids*; Oxford University Press: New York, 1999; p 309.